Cortical and subcortical mapping of the allostatic-interoceptive system in the human brain: replication and extension with 7 Tesla fMRI

Jiahe Zhang[1], Danlei Chen[1], Tara Srirangarajan[2], Jordan Theriault[3], Philip A. Kragel[4], Ludger Hartley[1], Kent M. Lee[1], Kieran McVeigh[1], Tor D. Wager[5], Lawrence L. Wald[3], Ajay B. Satpute[1], Karen S. Quigley,[1] Susan Whitfield-Gabrieli[1], Lisa Feldman Barrett[1,3,6]* & Marta Bianciardi[3,7]*

[1] Department of Psychology, Northeastern University, Boston, MA 02115
[2] Department of Psychology, Stanford University, Stanford, CA 94305
[3] Department of Radiology, Athinoula A. Martinos Center for Biomedical Imaging, Massachusetts General Hospital and Harvard Medical School, Boston, MA 02139
[4] Department of Psychology, Emory University, Atlanta, GA 30322
[5] Department of Psychological and Brain Sciences, Dartmouth College, Hanover, NH 03755
[6] Department of Psychiatry, Massachusetts General Hospital and Harvard Medical School, Boston, MA 02139
[7] Division of Sleep Medicine, Harvard University, Boston, MA

*L.F.B. and M.B. share senior authorship.

Corresponding Authors:
Jiahe Zhang, Department of Psychology, 125 Nightingale Hall, Northeastern University, Boston, MA 02115-5000. Email: j.zhang@northeastern.edu
Lisa Feldman Barrett, Department of Psychology, 125 Nightingale Hall, Northeastern University, Boston, MA 02115-5000. Email: l.barrett@northeastern.edu
Marta Bianciardi, Department of Radiology, Athinoula A. Martinos Center for Biomedical Imaging, Massachusetts General Hospital and Harvard Medical School, Building 149, Room 2301, 13th Street, Charlestown, MA 02129. Email: martab@mgh.harvard.edu

Author contributions: T.W., L.W., A.B.S., L.F.B. and M.B. designed research. J.Z., D.C., J. T., L.H., K.M.L, K.M., A.B.S., K.S.Q., S.W-G., L.F.B. and M.B. performed research. J.Z., D.C., T.S., L.F.B. and M.B. analyzed data and wrote the paper. All authors read and approved the paper.

Competing interest statement: The authors declare no conflict of interest.

Classification: Biological Sciences/Neuroscience

Keywords: visceromotor, interoception, viscerosensory, predictive coding

Abstract (250 words max)
The brain continuously anticipates the energetic needs of the body and prepares to meet those needs before they arise, a process called allostasis. In support of allostasis, the brain continually models the internal state of the body, a process called interoception. Using published tract-tracing studies in non-human animals as a guide, we previously identified a large-scale system supporting allostasis and interoception in the human brain with functional magnetic resonance imaging (fMRI) at 3 Tesla. In the present study, we replicated and extended this system in humans using 7 Tesla fMRI ($N = 91$), improving the precision of subgenual and pregenual anterior cingulate topography as well as brainstem nuclei mapping. We verified over 90% of the anatomical connections in the hypothesized allostatic-interoceptive system observed in non-human animal research. We also identified functional connectivity hubs verified in tract-tracing studies but not previously detected using 3 Tesla fMRI. Finally, we demonstrated that individuals with stronger fMRI connectivity between system hubs self-reported greater interoceptive awareness, building on construct validity evidence from our earlier paper. Taken together, these results strengthen evidence for the existence of a whole-brain system supporting interoception in the service of allostasis and we consider the implications for mental and physical health.

Significance Statement (120 words max)
We used ultra-high field 7 Tesla fMRI to replicate and extend a large-scale brain system supporting interoception and allostasis, entwined processes crucial to the core brain function of coordinating and regulating the internal systems of the body. In particular, we mapped the subcortical extents of this system, several of which are small brainstem nuclei only recently delineated at 7 Tesla. Our findings suggest that investigations of distributed brain networks should not be restricted to the cerebral cortex. We emphasize bodily regulation as a whole-brain phenomenon and highlight its implications for mental and physical health.

Introduction

A key function of a brain is to efficiently regulate and coordinate the systems of the body as an organism continually interfaces with an ever-changing and only partly predictable world. Various lines of research, including tract-tracing studies of non-human animals (e.g., 1, 2), discussions of predictive processing (3–6), and research on the central control of autonomic nervous system function (7–9) all suggest the existence of a unified, distributed brain system that anticipates the metabolic needs of the body and prepares to meet those needs before they arise, a process called allostasis (10; for recent reviews, see 11, 12). Allostasis is not a condition or state of the body — it is the process by which the brain efficiently maintains energy balance in the service of metabolic regulation (10). Just as somatosensory and other exteroceptive sensory signals are processed in the service of skeletomotor control, the brain is thought to model the internal sensory state of the body (i.e., the internal milieu) in the service of allostasis, a process known as interoception (13–16). In 2017, we identified a distributed allostatic-interoceptive system consisting of two overlapping intrinsic networks (**Figure 1A**), using resting state functional magnetic resonance imaging (rs-fMRI) in three samples with over 600 human subjects scanned at 3 Tesla (17). Our investigation was guided by the anatomical tracts identified in studies of non-human mammals (see Table 2 in (17)). Specifically, we examined the functional connectivity of primary interoceptive cortex spanning the dorsal mid and dorsal posterior insula (dmIns/dpIns), as well as key allostatic regions that are known to be responsible for controlling the motor changes in the viscera (i.e., visceromotor regions), such as the anterior midcingulate cortex (aMCC), pregenual anterior cingulate cortex (pACC), subgenual anterior cingulate cortex (sgACC), agranular insular cortex (also known as ventral anterior insula, or vaIns, which is also posterior orbitofrontal cortex), and dorsal amygdala (dAmy) (**Figure 1A**). This analysis yielded an integrated system consisting of two well-known intrinsic networks, the default mode network and salience networks, overlapping in connecting hubs, many of which are key cortical visceromotor allostatic regions that also serve as 'rich club' hubs, in addition to primary interoceptive cortex. We also probed the system's connectivity to some subcortical regions known to play a role in control of the autonomic nervous system, the immune system, and the endocrine system such as the thalamus, hypothalamus, hippocampus, ventral striatum, periaqueductal gray (PAG), parabrachial nucleus (PBN) and nucleus tractus solitarius (NTS; e.g., 18–24). The allostatic-interoceptive system has become an increasingly important tool for investigating interoception and allostasis processes under specific scenarios and in specific populations (e.g., (25–28)). In addition, research indicates that regions in this unified allostatic-interoceptive system are also important for a wide range of psychological phenomena that span cognitive, emotional, pain, decision-making and perceptual domains (see Figure 5 in (17); also see (29–31)), suggesting the hypothesis that allostatic and interoceptive signals may play a role in shaping brain dynamics and cognition (for discussion see (5, 32).

In the present study, we replicated and extended evidence for the allostatic-interoceptive system (**Figure 1B**) using ultra-high field (7 Tesla) MRI, which allows data acquisition with higher spatial resolution (1.1 mm isotropic), better signal-to-noise-ratio (SNR; Sclocco et al., 2018; Bandettini et al., 2012; Newton et al., 2012), and increased sensitivity in mapping functional connectivity of brainstem nuclei involved in arousal, motor and other vital processes (e.g., autonomic, nociceptive, sensory; 33). We tested within-system functional connectivity in 91 human participants (age range = 18-40, mean = 26.9, SD = 6.2 years old; 41 females, 50 males) using a fast low-angle excitation echo-planar technique (FLEET) sequence, which has been shown to reduce artifacts and improve temporal SNR (Polimeni et al., 2016; Kragel et al., 2019). This approach allowed a more precise mapping of connectivity for regions with known signal issues at 3 Tesla, such as the sgACC (low SNR), amygdala (noise from adjacent veins; (34)), columns within the PAG (noise from adjacent aqueduct), and other small structures that could be particularly influenced by partial volume effects. We took advantage of recently developed and much improved in-vivo brainstem and diencephalic nuclei atlases (35–39) to guide our hypotheses (**Table S1**), which were derived from tract-tracing studies of non-human mammals. Building on (17), we specifically examined the connectivity to subcortical nuclei such as the NTS (in the medullary viscero-sensory-motor

nuclei complex; VSM), dorsal raphe (DR), substantia nigra (SN), ventral tegmental area (VTA), locus coeruleus (LC), superior colliculus (SC), mediodorsal thalamus (mdThal), and lateral geniculate nucleus (LGN). While SC and LGN are not traditionally considered directly involved in interoception and allostasis, they share anatomical connections with key visceromotor regulation regions in the network (see **Table S1**; (40–45)). SC has been directly implicated in skeletomotor (46, 47) and visceromotor (48, 49) actions that facilitate approach or avoidance behaviors. SC is also thought to integrate sensory information to generate a representation of the body, which then gives rise to basic, valenced feelings (50, 51). We also examined connectivity patterns for subregions of the PAG, hippocampus and SC rather than as a single ROI as in (16) given their functional heterogeneity (52, 53) and differential involvement in allostasis (e.g., (54–56)).

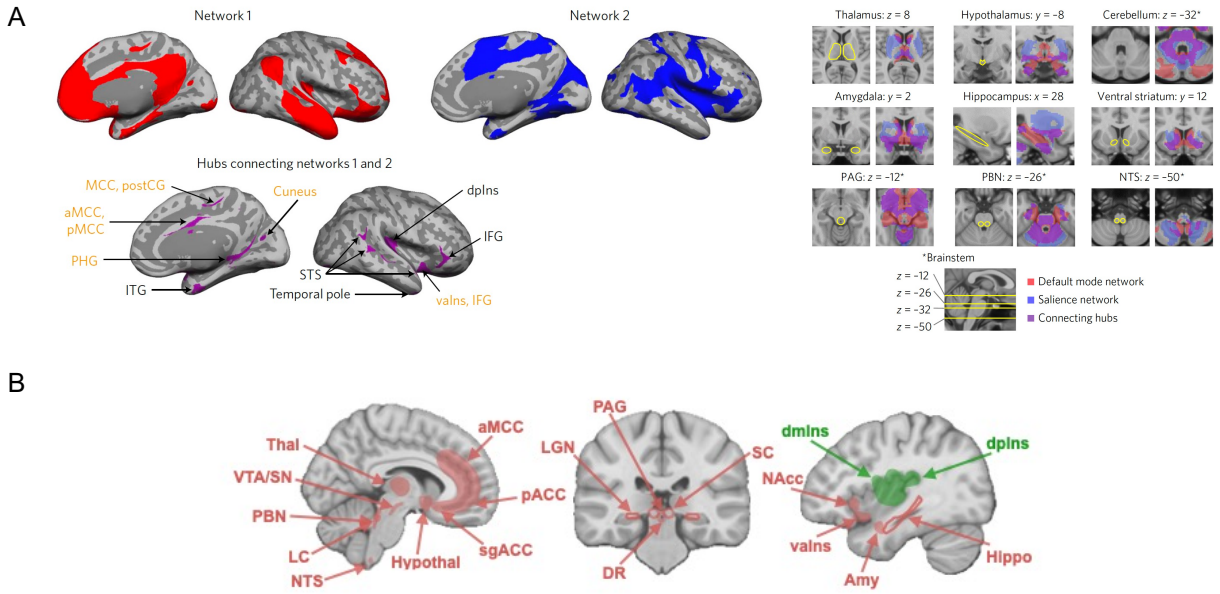

Figure 1. Key cortical and subcortical regions involved in interoception and allostasis. **(A)** Using 3 Tesla fMRI resting state connectivity, we showed a unified system consisting of the default mode network (in red) and salience network (in blue), which overlapped in connecting hubs (in purple), many of which are key cortical visceromotor allostatic regions that also serve as 'rich club' hubs, in addition to a portion of primary interoceptive cortex (dpIns) (left panel) (17). We reported the system's connectivity to some subcortical regions known to play a role in control of the autonomic nervous system, the immune system, and the endocrine system such as the thalamus, hypothalamus, hippocampus, ventral striatum, PAG, PBN and NTS (e.g., 18–24) (right panel) (17). Figures are reproduced with permission from (17). (B) Expanded set of seed regions used in the present analysis. Abbreviations: aMCC: anterior midcingulate cortex; Amy: amygdala; dmIns: dorsal mid insula; dpIns: dorsal posterior insula; DR: dorsal raphe; Hippo: hippocampus; Hypothal: hypothalamus; LC: locus coeruleus; LGN: lateral geniculate nucleus; NAcc: nucleus accumbens; NTS: nucleus of the solitary tract; pACC: pregenual anterior cingulate cortex; PAG: periaqueductal gray; PBN: parabrachial nucleus; SC: superior colliculus; sgACC: subgenual anterior cingulate cortex; SN: substantia nigra; Thal: thalamus; vaIns: ventral anterior insula; VTA: ventral tegmental area.

Results

Following the analytic methods reported in (17), we opted to separate signal from random noise using replication according to the mathematics of classical measurement theory (57) rather than stringent statistical thresholds that can cause Type II errors (58). We randomly divided the sample into two subsamples (*Ns* = 46 and 45) and identified, for each seed region, BOLD correlations for all voxels in the brain that survived a voxel-wise threshold of $p < .05$ across both subsamples. Each subsample produced a

set of discovery maps for each seed region that included both cortical and subcortical connections. The maps of each subsample were subjected to *k*-means clustering analysis to estimate the allostatic-interoceptive network. This approach allowed us to identify weak but reliable signals that are important when examining cortico-subcortical connections in brain-wide analyses. We expected stronger connectivity among cortical seeds compared to among subcortical seeds due to noisier time courses and more partial volume effects resulting in lower sensitivity in smaller regions.

Cortico-cortical intrinsic connectivity. The two subsamples demonstrated high between-sample reliability for cortical connectivity profiles of all cortical seeds (η^2 mean = 0.92, s.d. = 0.03) (59). We first examined the hypothesized functional connectivity based on documented anatomical connections. As expected, we successfully replicated all of the cortico-cortical connections observed with 3 Tesla imaging reported in (17). We additionally observed reciprocal connectivity (i.e., connectivity map of one region includes a cluster in the other region and vice versa) between lvAIns and pACC, between sgACC and aMCC, and between dmIns and portions of cingulate cortex (sgACC, pACC) (subsample 1, **Figure 2A**; subsample 2, **Figure S1A**), extending the system to include more connections predicted by animal tract-tracing studies ((60–63)). These observations were confirmed by seed-to-seed connectivity strength calculation (subsample 1, **Figure 2B**; subsample 2, **Figure S1B**). Combining evidence from the cortical maps and seed-to-seed connectivity matrices, we confirmed 100% of the monosynaptic cortico-cortical connections predicted from non-human tract-tracing studies.

Next, to identify connecting cortical hubs, we binarized the cortical connectivity maps for all cortical seeds ($p < 0.05$) and computed their conjunction (subsample 1, **Figure 2C**; subsample 2, **Figure S1C**), which allowed for discovery of important regions outside the hypothesized seeds. We replicated all the hubs reported at 3 Tesla in (17) with the exception of medial postcentral gyrus, and we newly identified the entire anterior cingulate cortex (including subgenual and pregenual extents), posterior cingulate cortex (PCC), a greater extent of the insula (including mid insula; mIns), as well as some portions of medial superior frontal gyrus (SFG) and middle frontal gyrus (MFG). A *k*-means clustering analysis ($k = 2$, 1000 iterations) on the cortical maps replicated two clusters that replicated the two-network system resembling the default mode network (i.e., the dorsomedial prefrontal cortex, PCC, and dorsolateral prefrontal cortex) and salience network (i.e., anterior to MCC, anterior insula, supramarginal gyrus, supplementary motor area; see details in **Figure S2**).

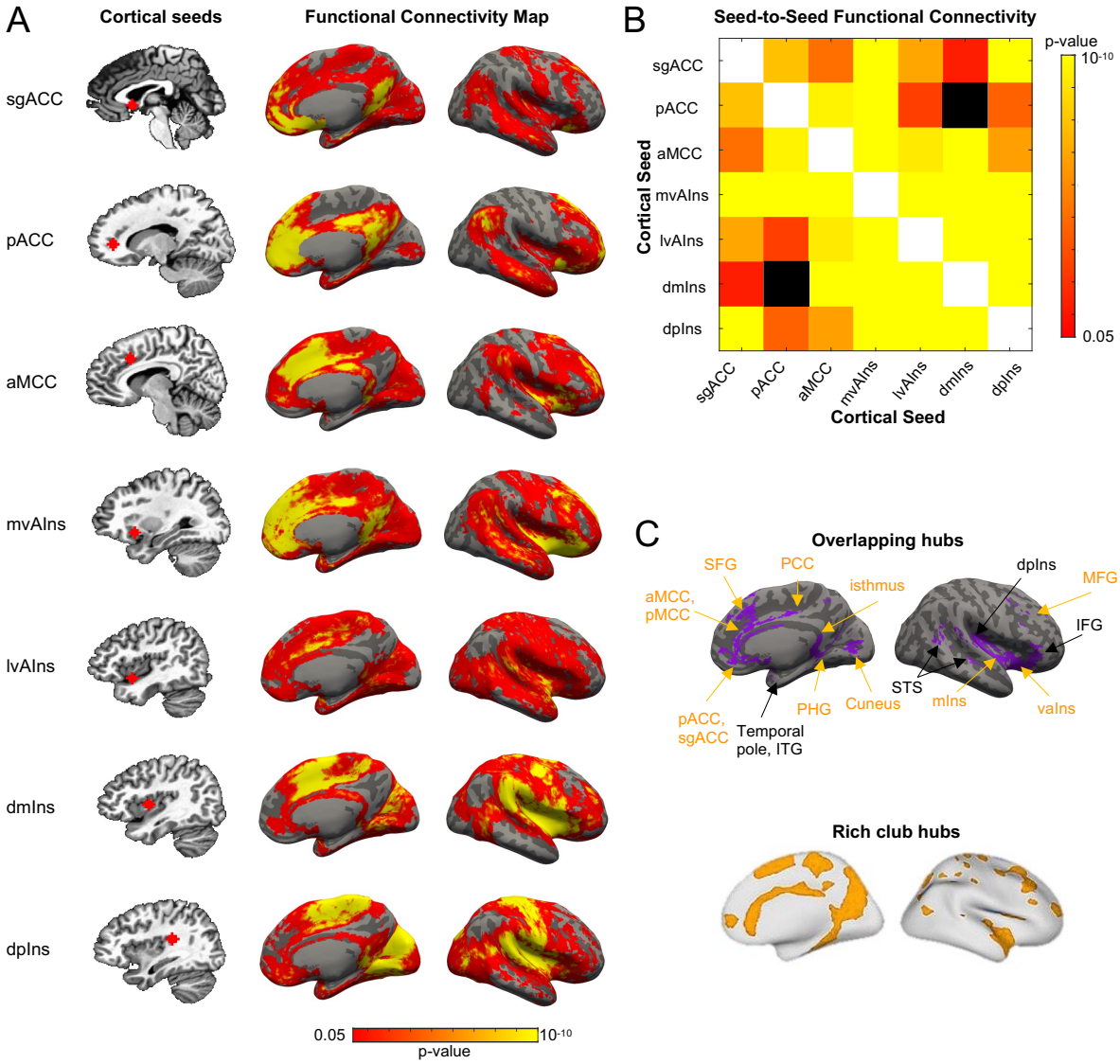

Figure 2. Cortico-cortical functional connectivity within the allostatic-interoceptive system in subsample 1. **(A)** Left column shows cortical seed locations and right column shows functional connectivity discovery maps depicting all voxels whose time course was correlated with that of the seed (ranging from $p < .05$ in red to $p < 10^{-10}$ in yellow, uncorrected, $N = 46$, medial and lateral view displayed on the left and right column, respectively). **(B)** Seed-to-seed functional connectivity matrix shows connectivity strength between each pair of the cortical seeds (ranging from $p < .05$ in red to $p < 10^{-10}$ in yellow, uncorrected; white color indicates correlation =1 and black color indicates subthreshold correlations; $N = 46$). Note that although pACC-dmIns connectivity strength did not meet threshold, a pACC cluster was observed in the dmIns-seeded map and a dmIns cluster was observed in the pACC-seeded map, in (**A**). **(C)** The allostatic-interoceptive system showed overlapping hubs in all the *a priori* interoceptive and visceromotor control regions. Hubs belonging to the 'rich club' are shown in yellow. 'Rich club' hubs figure adapted with permission from (64). To avoid Type II errors, which are enhanced with the use of stringent statistical thresholds (58), we opted to separate signal from random noise using replication, according to the mathematics of classical measurement theory (57). The above results were replicated in a second subsample, $N = 45$, indicating that they are reliable and cannot be attributed to random error (**Figure S1**). Abbreviations: aMCC: anterior mid cingulate cortex; dpIns: dorsal posterior insula; IFG: inferior frontal gyrus; MFG: middle frontal gyrus; mIns: mid insula; pACC: pregenual anterior cingulate cortex; PHG: parahippocampal gyrus; pMCC: posterior mid cingulate cortex; PCC: posterior cingulate cortex; sgACC: subgenual anterior cingulate cortex; STS: superior temporal sulcus; vaIns: ventral anterior insula.

Subcortico-cortical intrinsic connectivity. Using a similar analysis strategy, we assessed subcortico-cortical connectivity by both visually inspecting cortical discovery maps of the subcortical seeds to confirm topography (subsample 1, **Figure 3A**; subsample 2, **Figure S3A**) as well as calculating seed-to-seed connectivity to quantify strength of connection (subsample 1, **Figure 3B**; subsample 2, **Figure S3B**). The two subsamples demonstrated high between-sample reliability (η^2 mean = 0.85, s.d. = 0.06). Combining evidence from the cortical maps and seed-to-seed connectivity matrix, we confirmed 98% of the monosynaptic subcortico-cortical connections predicted from non-human tract-tracing studies; the one exception was we did not observe functional connectivity between PAG and dmIns/dpIns despite known anatomical connections (65, 66). Note that in some instances, averaged timecourses between seeds did not correlate significantly (i.e., black squares in matrix, e.g., PAG-pACC), but connectivity clusters could nonetheless be observed in the maps (e.g., pACC cluster in PAG-seeded map). These discrepancies can result from noisy signals within an ROI or specific sub-portions of an ROI showing significant connectivity. We also observed one aspect of relative specificity: a region of superior parietal lobule (not known for visceromotor function) with tract-tracing-based connections only to the SC (67) showed consistent functional connectivity to the SC as well as to two large subcortical hubs (the hippocampus and the amygdala) (**Table S2**).

Subregions of the PAG delineated with diffusion weighted imaging (**Figure S4**; see Supplementary Information for more details) showed largely similar functional connectivity profiles overall, although lPAG and vlPAG showed more robust and more extensive connectivity than dmPAG and dlPAG, with stronger connectivity especially with aMCC and mvAIns (**Figure S5**), mirroring previously reported shift in functional organization in the rostrocaudal axis (52, 56). Longitudinal functional subdivisions of the hippocampus into head, body, and tail (51; see Supplementary Information for more details) also showed largely similar functional connectivity profiles, albeit with a gradient from greater connectivity to the default mode network at the anterior end and greater connectivity to the salience network at the posterior end (**Figure S6**), consistent with prior work (68, 69). Both rostrolateral and caudomedial subregions of the SC (corresponding to superficial and intermediate/deep layers) showed similar connectivity to cortical regions affiliated with the default mode-like portion of the unified system, whereas the rostrolateral subregion alone showed stronger connectivity to cortical regions affiliated with the salience-like portion of the system (**Figure S7**, **Table S3**).

Next, we conjoined the binarized discovery maps ($p < 0.05$) to identify the cortical hubs in each subsample where subcortical connections overlapped (subsample 1, **Figure 3C**; subsample 2, **Figure S3C**). This analysis was enabled by newly delineated subcortical seeds (36, 39, 70) and therefore was not possible at 3 Tesla (17). Similar to the cortically seeded maps, subcortically seeded maps showed connecting hubs in hypothesized cingulate and insular regions as well as some parts of the MFG and cuneus. We ran k-means clustering analysis ($k = 2$) (subsample 1: frequency = 734/1000, adjusted Rand index = 0.61; subsample 2: frequency = 897/1000, adjusted Rand index = 0.81) which appeared to differentiate maps showing sparse connectivity from those showing more widespread (dense) connectivity rather than differentiating spatially distinct connectivity patterns (sparse: Cluster 1 from maps seeded in the hypothalamus, PAG, DR, PBN, LC and VSM; dense: Cluster 2 seeded in the mdThal, LGN, hippocampus, dAmy, NAcc, SC, SN and VTA; Cluster 2, **Figure S8**). These two clusters could reflect a meaningful functional difference (e.g., central nodes of the network may show widespread connectivity) and/or methodological limitations (e.g., poorer SNR in smaller regions may lead to sparse connectivity).

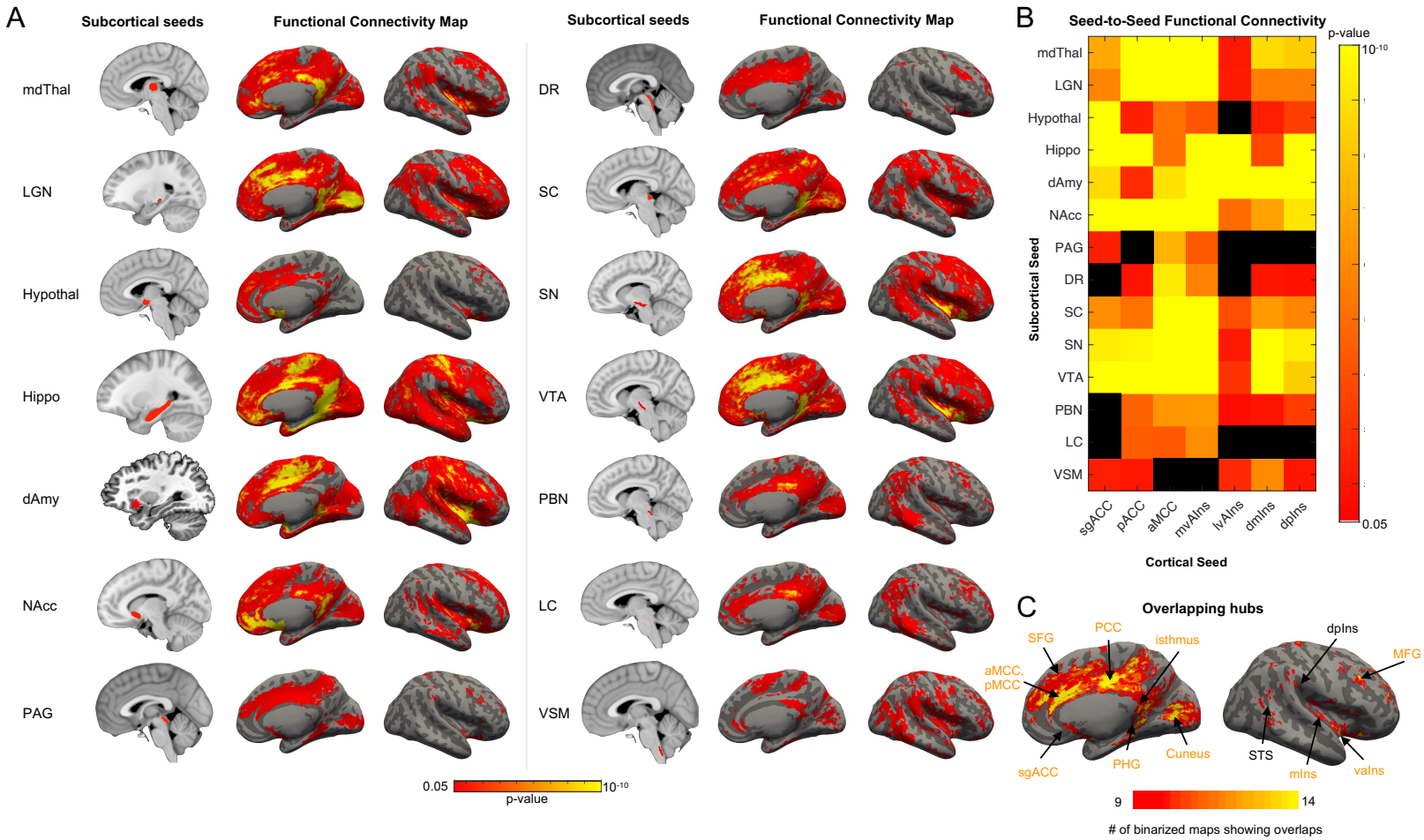

Figure 3. Subcortico-cortical intrinsic connectivity within the allostatic-interoceptive system in subsample 1. **(A)** Left column shows subcortical seed locations and right column shows functional connectivity discovery maps depicting all cortical voxels whose time course was correlated with that of the seed (ranging from $p < .05$ in red to $p < 10^{-10}$ in yellow, uncorrected, $N = 46$). **(B)** Seed-to-seed functional connectivity matrix shows connectivity strength between pairs of subcortical and cortical seeds (ranging from $p < .05$ in red to $p < 10^{-10}$ in yellow, uncorrected; white color indicates correlation =1 and black color indicates subthreshold correlations; $N = 46$). **(C)** Conjunction map shows the number of binarized maps ($p < .05$) that overlap at the connecting hubs (ranging from 9 to 14). The above results were replicated in a second subsample, $N = 45$, indicating that they were reliable and could not be attributed to random error (**Figure S3**). Abbreviations: dAmy: dorsal amygdala; mdThal: mediodorsal thalamus; LGN: lateral geniculate nucleus; Hypothal: hypothalamus; Hippo: hippocampus; NAcc:

nucleus accumbens; PAG: periaqueductal gray; DR: dorsal raphe; SC: superior colliculus; SN: substantia nigra; VTA: ventral tegmental area; PBN: parabrachial nucleus; LC: locus coeruleus; VSM: medullary viscero-sensory-motor nuclei complex corresponding to the nucleus tractus solitarius.

Subcortico-subcortical intrinsic connectivity. We assessed subcortico-subcortical connectivity by both visually inspecting subcortical maps of the subcortical seeds to confirm topography as well as calculating functional connectivity between all subcortical seeds to quantify strength of connection (subsample 1, **Figure 4**; subsample 2, **Figure S9**). Again, this analysis was not possible with 3 Tesla scanning as in (18). We confirmed 100% of the monosynaptic subcortico-subcortical connections that were predicted from non-human tract-tracing studies. Note that in some instances, averaged timecourses between seeds did not correlate significantly (i.e., black squares in matrix, e.g., DR-hypothalamus), but connectivity clusters could nonetheless be observed in the maps (e.g., hypothalamus cluster in DR-seeded map). These discrepancies can result from noisy signals within an ROI or specific sub-portions of an ROI showing significant connectivity. Seed-to-seed connectivity strength between PAG subregions and other subcortical ROIs is displayed in **Figure S5**. Seed-to-seed connectivity strength between hippocampal subregions and other subcortical ROIs is displayed in **Figure S6**. Seed-to-seed connectivity strength between SC layers and other subcortical ROIs is displayed in **Figure S7**. Conjoined binarized subcortical discovery maps ($p < 0.05$) indicated that all but four subcortical seeds showed hub-like connectivity (hubs identified in the mdThal, LGN, hippocampus, dAmy, NAcc, PAG, DR, SC, SN and VTA but hypothalamus, PBN, LC and VSM showed less widespread and dense connectivity throughout subcortical seeds (**Table S4**). K-means clustering analysis ($k = 2$) on the subcortical discovery maps from subcortical seeds yielded an almost identical solution as their cortical connectivity maps (subsample 1: frequency = 734/1000, adjusted Rand index = 0.61; subsample 2: frequency = 897/1000, adjusted Rand index = 0.81). The only difference was that the hypothalamus switched membership from Cluster 1 to Cluster 2 despite it being a major visceromotor structure with evident anatomical connections to all subcortical regions.

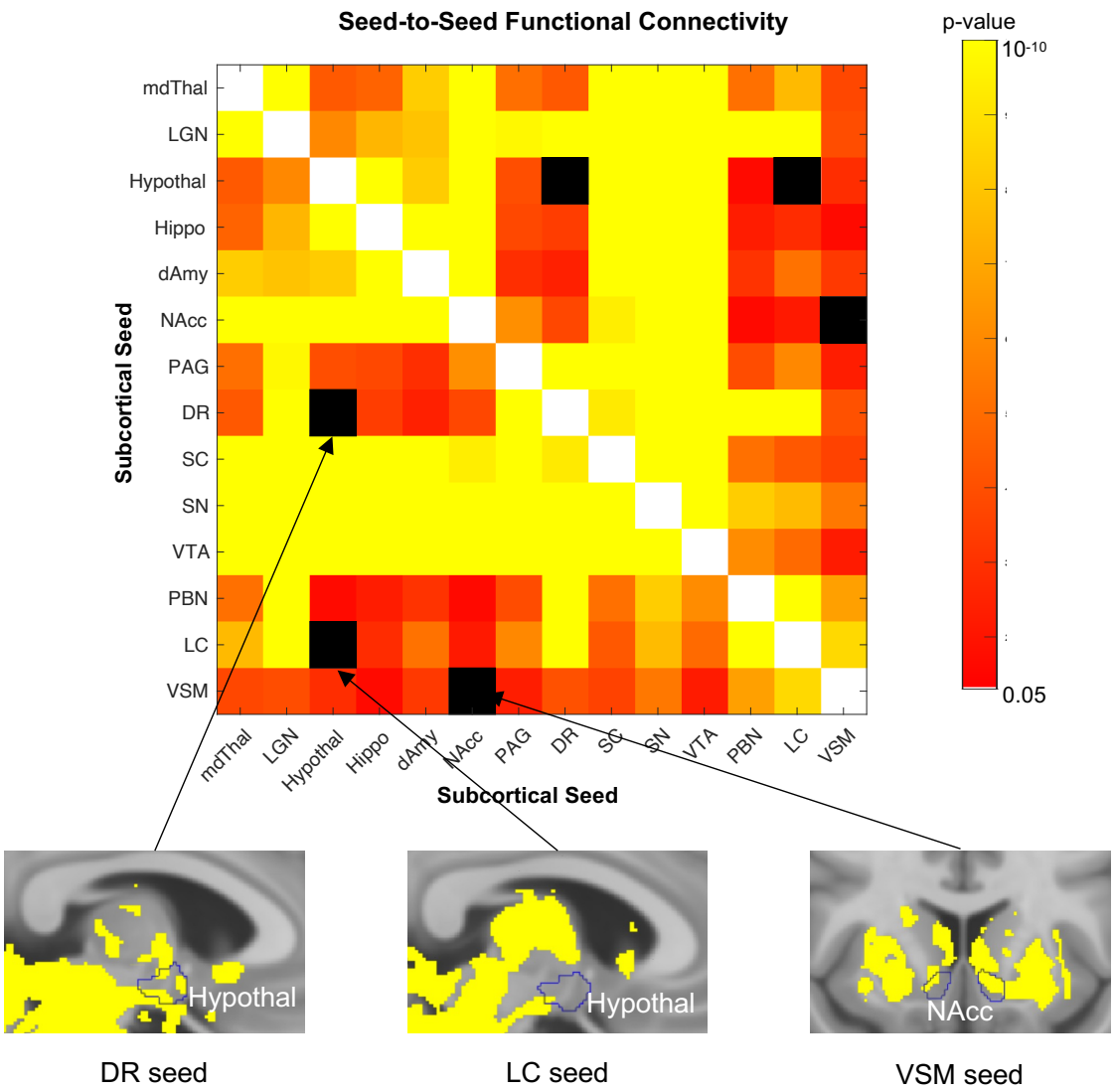

Figure 4. Subcortico-subcortical intrinsic connectivity within the allostatic-interoceptive system in subsample 1. Seed-to-seed functional connectivity matrix showed connectivity strength between each pair of the subcortical seeds (ranging from $p < .05$ in red to $p < 10^{-10}$ in yellow, uncorrected; white color indicates correlation =1 and black color indicates subthreshold correlations; $N = 46$). Several seeds had functional connectivity with a subset of voxels within target ROIs, as shown by binarized maps at $p < .05$ (target ROI outline is shown in blue). The above results were replicated in a second subsample, $N = 45$, indicating that they were reliable and could not be attributed to random error (**Figure S9**).

The allostastic-interoceptive system. We observed dense interconnectivity between all the seeds included in our analysis (subsample 1: **Figure 5A**; subsample 2: **Figure S10A**). Combining both cortical and subcortical extents, functional connectivity of the seeds converged in the hypothesized allostatic-interoceptive system (subsample 1: **Figure 5B**; subsample 2: **Figure S10B**).

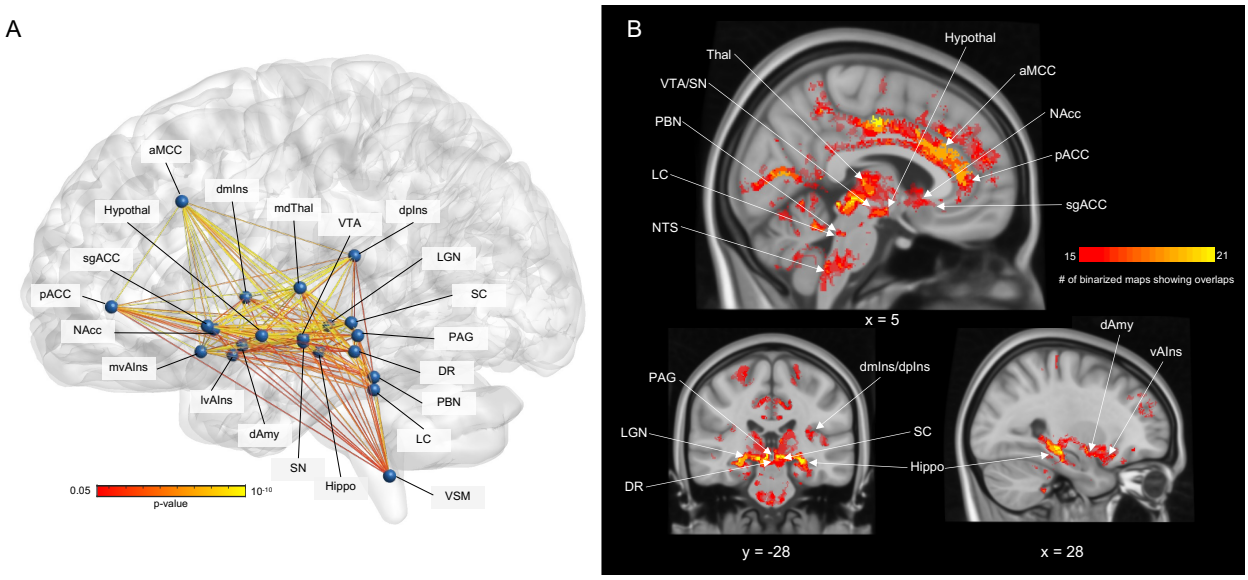

Figure 5. Summary of the allostatic-interoceptive system based on 7 Tesla fMRI functional connectivity in subsample 1. **(A)** Circuit diagram indicates dense within-system connectivity between the 21 cortical and subcortical seeds. All seeds are shown as spherical nodes located at their respective centers of gravity. Pairwise connectivity strengths between ROIs are shown as edges between nodes (ranging from $p < .05$ in red to $p < 10^{-10}$ in yellow, uncorrected, $N = 46$). Nodes and edges in the glass brain were visualized using BrainNet Viewer (71) **(B)** Conjunction map shows the number of binarized maps ($p < .05$) that overlapped at the connecting hubs (ranging from 15 to 21, total number of cortical and subcortical seeds = 21). The above results were replicated in a second subsample, $N = 45$, indicating that they were reliable and could not be attributed to random error (**Figure S10**).

Construct Validity. Finally, we conceptually replicated a previously reported association between interoceptive ability and functional connectivity strength between the dpIns (primary interoceptive cortex) and aMCC (an *a priori* visceromotor region and a connector hub, with consistently replicated tract-tracing connectivity to subcortical allostatic nuclei) (18). To avoid Type II error resulting from multiple comparison correction, we computed intrinsic functional connectivity between the same two seeds (i.e., dpIns and aMCC) and found that individuals showing stronger intrinsic dpIns-aMCC functional connectivity also reported greater self-reported interoceptive awareness ($r = 0.24$, $p < 0.023$; **Figure S11**).

Discussion (1500 words max)

Ultra-high field 7 Tesla fMRI with 1.1-mm isotropic voxel resolution combined with newly delineated 7 Tesla brainstem and diencephalic parcellations (35–39) allowed us to replicate and extend both the cortical and subcortical components of the allostatic-interoceptive system originally identified in humans with 3 Tesla fMRI (17). Our original study involved 10-minute resting state scans in two subsamples of 270-280 participants each, whereas the present study involved longer, 30-minute resting state scans in two subsamples of 45-46 participants each. With seven cortical ROIs and 14 subcortical ROIs, we verified over 90% of the anatomical connections identified in published tract-tracing studies in non-human mammals using functional connectivity in humans. Our current 7 Tesla findings revealed reciprocal connectivity between sgACC/pACC and dmIns/dpIns regions previously unreported in 3 Tesla functional connectivity studies of the ACC (72–76) and the insula (77–80). The improvement in sgACC connectivity, in particular, was expected at 7 Tesla, as this region is part of the medial/orbital surface that is typically susceptible to low SNR, partial volume effects and physiological aliasing; in the current study, these effects were mitigated by higher resolution image acquisition at 7 Tesla, minimal smoothing, and more precise nuisance regression using signals from individual ventricles. We also expanded observations of the subcortical extents of the allostatic-interoceptive system. Several subcortical nodes (i.e., mdThal, LGN, hippocampus, dAmy, NAcc, SC, SN and VTA) showed robust connectivity with all cortical nodes

whereas the smaller brainstem nuclei (i.e., PAG, DR, PBN, LC and VSM) showed weaker but reliable connectivity to these nodes, replicating earlier findings using a subset of the nodes as seeds at 3 Tesla (e.g., (81)) and 7 Tesla (e.g., (33, 82)). We also observed reliable connectivity between regions that have not yet been documented as having monosynaptic connections in previous tract-tracing studies. For example, anatomical evidence shows limited monosynaptic connectivity between the LGN and cortical nodes of the system (except pACC), yet we observed reliable functional connectivity between the LGN and both the aMCC and mvAIns (as well as the pACC). This finding requires further investigation because our estimate of functional connectivity was likely sensitive to polysynaptic connections.

In addition, the connecting hubs of the allostatic-interoceptive system observed at 7 Tesla covered *all* hypothesized cortical regions of interest, including the extent of primary interoceptive cortex (dpIns, dmIns) and visceromotor allostatic regions in the vAIns, sgACC, pACC and aMCC. Several other connecting hubs (MCC, PCC, IFG, PHG, STG) were also observed and had confirmed anatomical connections to hypothesized allostatic-interoceptive regions in non-human animals (2, 65, e.g., 83–86). The remaining connecting hubs (i.e., MFG, SFG, isthmus of the cingulate, cuneus) did not have evident monosynaptic anatomical connections to the hypothesized regions – their functional connectivity may reflect polysynaptic connections or novel connections in humans (e.g., MFG and SFG do not have homologous counterparts in non-human animals). Importantly, most of the additional connecting hubs observed at 7 Tesla (i.e., pACC, PCC, isthmus cingulate, SFG, MFG and mIns; except the sgACC) belong to the 'rich club' (the most densely interconnected regions in the cortex) (64), consistent with the hypothesized central role of the allostatic-interoceptive system as a high-capacity backbone for integrating information across the entire brain (87).

We did not map every possible subcortical area that may be involved in allostasis or interoception. For example, opportunities for further research include septal nuclei (with direct projections to limbic regions such as the hippocampus and implicated in temporal control of neurons that make up the allostatic-interoceptive work; (88, 89)), circumventricular organs (e.g., area postrema with unique access to peripheral signaling molecules via its permeable blood-brain-barrier; (90, 91)) and motor brainstem nuclei (e.g., dorsal motor nucleus of the vagus and nucleus ambiguus whose neurons give rise to the efferent vagus nerve; (92, 93)).

The results of this study have several important functional implications. First, several brain regions within the allostatic-interoceptive network may play an important role in coordinating and regulating the systems of the body even though they are typically assigned other psychological functions. For example, the SC is typically studied for visuomotor functioning in humans but has been shown to be important for approach and avoidance behavior as well as the accompanying changes in visceromotor activity in non-human mammals (e.g., 48, 49, 94) via anatomical connections to ACC (40) and hypothalamus (41). Similarly, the hippocampus is usually considered central to memory function, but evidence from non-human animals indicates that the hippocampus also plays a role in interoceptive processing in feeding behaviors and interoception-related reward signals (95–99). There is also circumstantial evidence that interoceptive signals, relayed from the vagus nerve to the hippocampus via the NTS and septal nuclei, may play a role in event segmentation (100, 101). The LGN is typically considered a part of the visual pathway that relays visual information from the retina and the cerebral cortex. However, the current functional connectivity findings are consistent with tract-tracing evidence showing LGN's anatomical connections with many visceromotor structures both cortically (e.g., pACC (102)) and subcortically (e.g., hypothalamus (103), PAG (42), and PBN (104)), suggesting a role for facilitating communication among brain structures implicated in bodily regulation, in addition to its role in integrating interoceptive and visual signals (32).

Second, a more mechanistic understanding of how the default mode and salience networks support interoception and allostasis will also reveal insights into the mind–body connections at the root of mental and physical illness and their comorbidities. Many psychiatric illnesses (e.g., depression (105, 106), schizophrenia (107, 108)), neurodevelopmental illnesses (e.g., sensory processing disorder/autism spectrum disorder (109, 110)), neurodegenerative illnesses (e.g., dementia/Alzheimer's disease (111, 112), Parkinson's disease (113, 114)) and physical illnesses (e.g., heart disease (115), chronic pain (116))

present with symptoms related to altered interoception or visceromotor control, and some of these symptoms are transdiagnostic (117–119). Interoceptive and visceromotor symptomatology is often accompanied by altered neurobiology (e.g., volume, structural connectivity, functional connectivity, evoked potential, task activation) in the allostatic-interoceptive system (e.g., depression: (120, 121); autism: (122); dementia: (26, 111, 112); chronic pain: (123); transdiagnostic: (124–127)). Accordingly, there is evidence showing that psychological therapies targeting interoceptive processes (128) and neuromodulations targeting distributed regions within the allostatic-interoceptive system (129, 130) may be effective transdiagnostic interventions. A unified cortical and subcortical system provides an anatomical and functional framework for integrating studies across psychological and illness domains in a manner that will speed discovery, the accumulation of knowledge and, potentially, strategies for more effective treatments and prevention.

Finally, the findings reported here are consistent with the growing body of evidence that subcortical and cortical brain regions are both important for the regulation of bodily functions and for so-called "higher" cognitive functions, calling into question the notion that there is an anatomical basis for segregating the two types of functions (115, 116). That the default mode and salience networks may be concurrently coordinating, regulating and representing the internal milieu, while they are routinely engaged in a wide range of tasks spanning cognitive, perceptual, emotion and action domains (see Figure 5 in (17)), all of which involve value-based decision-making and action (31, 133–137) reinforces the viability of the hypothesis that, whatever other psychological functions the default mode and salience networks are performing during any given brain state, they are simultaneously maintaining or attempting to restore allostasis and are integrating sensory representations of the internal milieu with the rest of the brain for the purposes of allostasis. Therefore, our results, when situated in the published literature, suggest that the default mode and salience networks create a highly connected functional ensemble for integrating information across the brain, with interoceptive and allostatic information at its core. Regulation of the body has been largely ignored in the neuroscientific study of the mind, in part because much of interoception occurs outside of human awareness (16, 118).

Materials and Methods

Participants and MRI acquisition. We recruited 140 native English-speaking adults, with normal or corrected-to-normal vision, and no history of neurological or psychiatric conditions. All participants provided written informed consent in accordance with the guidelines set by the institutional review board of Massachusetts General Hospital. Nineteen participants withdrew from the study prior to the MRI session, 12 withdrew during MRI acquisition, four were excluded due to technical issues during acquisition, and 14 were excluded due to poor data quality (assessed by visual inspection) or high motion. This resulted in a final sample of 91 participants (26.9 ± 6.2 years old; 41 females, 50 males). MRI data were acquired using a 7 Tesla scanner (Magnetom, Siemens Healthineers, Erlangen, Germany) with a 32-channel phased-array head coil. Participants completed a structural scan, three resting state scans, three diffusion-weighted scans, the Kentucky Inventory of Mindfulness Skills (138), as well as other tasks unrelated to the current analysis. MRI parameters are detailed in SI.

Preprocessing of fMRI data. The preprocessing pipeline began with reorientation, slice timing correction, concatenation of all three resting state runs, coregistration to the structural T1-weighted image, and motion correction. We then conducted nuisance regression to remove physiological noise due to motion, as well as due to non-BOLD effects evaluated in the white matter, ventricular cerebrospinal fluid, and the cerebral aqueduct. We then conducted temporal filtering and normalization. Finally, we performed conversion to Freesurfer orientation/dimensions, detrending, spatial smoothing (1.25mm), and resampling to cortical surfaces. Preprocessing details are provided in SI.

Functional Connectivity Analysis. Seven cortical and 14 subcortical seeds were defined based on previous studies, standard atlases, and group probabilistic map. Subjects were randomly divided into a subsample 1 (N = 46) and a subsample 2 (N = 45). In each group, for each seed, we estimated cortical connectivity

using Freesurfer-based analysis procedure as outlined in (17). This yielded final group maps that showed regions whose fluctuations significantly correlated with the seed's fMRI time series. We also quantified seed-to-seed functional connectivity by computing Pearson's correlation coefficient between all pairs of ROIs and applying the Fisher's *r*-to-*z* transform. Significance at the group level was assessed with a two-tailed one-sample t test.

Reliability Analyses. We used η^2 as a reliability index because it shows similarity between maps while discounting scaling and offset effects (59). An η^2 value of 1 indicates spatially identical maps while an η^2 of 0 indicates no similarity. For each of our seeds, we calculated η^2 between the two subsamples using the effect size (gamma) maps generated by the group-level general linear model analysis. Then we calculated the mean and standard deviation of the η^2 across all seeds to index overall similarity between subsamples.

Connecting Hubs and K-Means Cluster Analysis. To visualize the connecting hubs, we conjoined all binarized group functional connectivity maps ($p < 0.05$). To replicate the previously discovered two-subsystem distinction within the allostatic-interoceptive network, we computed a similarity matrix capturing pairwise η^2 (59) between the group maps and applied k-means clustering algorithm (*kmeans*, MATLAB) with $k = 2$. To visualize each subsystem, we binarized the group connectivity maps ($p < 0.05$) and calculated the conjunction between maps within the same cluster.

Behavioral Validation. Participants self-reported on the Kentucky Inventory of Mindfulness Skills (138). We correlated the total scores from five interoceptive awareness items with functional connectivity strength (Fisher's *z*) between the primary interoceptive cortex (dpIns and dmIns) and a representative visceromotor region (aMCC).

Data and Code Accessibility. Connectivity maps can be found at: https://osf.io/8w9zp. Custom data processing and analysis codes are available upon request.

Acknowledgments:
This work was supported by grants from the National Institutes of Health (NCI U01 CA193632, R01 AG071173, R01 MH109464, R01 MH113234, NIDCD R21 DC015888, NIBIB K01 EB019474, and NIA R01 AG063982), the National Science Foundation (BCS 1947972), the U.S. Army Research Institute for the Behavioral and Social Sciences (W911NF-16-1-019), and the Unlikely Collaborators Foundation. The views, opinions, and/or findings contained in this review are those of the authors and shall not be construed as an official Department of the Army position, policy, or decision, unless so designated by other documents, nor do they necessarily reflect the views of the Unlikely Collaborators Foundation.

References

1. H. Barbas, N. Rempel-Clower, Cortical structure predicts the pattern of corticocortical connections. *Cerebral Cortex* **7**, 635–646 (1997).

2. D. Ongür, A. T. Ferry, J. L. Price, Architectonic subdivision of the human orbital and medial prefrontal cortex. *J Comp Neurol* **460**, 425–449 (2003).

3. L. F. Barrett, W. K. Simmons, Interoceptive predictions in the brain. *Nat Rev Neurosci* **16**, 419–429 (2015).

4. K. Friston, T. FitzGerald, F. Rigoli, P. Schwartenbeck, G. Pezzulo, Active Inference: A Process Theory. *Neural Computation* **29**, 1–49 (2017).

5. J. B. Hutchinson, L. F. Barrett, The Power of Predictions: An Emerging Paradigm for Psychological Research. *Current Directions in Psychological Science* **28**, 280–291 (2019).

6. H. Straka, J. Simmers, B. P. Chagnaud, A New Perspective on Predictive Motor Signaling. *Curr Biol* **28**, R232–R243 (2018).

7. E. E. Benarroch, The Central Autonomic Network: Functional Organization, Dysfunction, and Perspective. *Mayo Clinic Proceedings* **68**, 988–1001 (1993).

8. P. J. Gianaros, T. D. Wager, Brain-Body Pathways Linking Psychological Stress and Physical Health. *Curr Dir Psychol Sci* **24**, 313–321 (2015).

9. G. Valenza, *et al.*, The central autonomic network at rest: Uncovering functional MRI correlates of time-varying autonomic outflow. *Neuroimage* **197**, 383–390 (2019).

10. P. Sterling, Allostasis: a model of predictive regulation. *Physiol Behav* **106**, 5–15 (2012).

11. P. Sterling, S. Laughlin, *Principles of Neural Design* (MIT Press, 2015).

12. Y. Katsumi, J. E. Theriault, K. S. Quigley, L. F. Barrett, Allostasis as a core feature of hierarchical gradients in the human brain. *Network Neuroscience*, 1–56 (2022).

13. A. D. Craig, How do you feel? Interoception: the sense of the physiological condition of the body. *Nature Reviews Neuroscience* **3**, 655–666 (2002).

14. A. D. Craig, *How Do You Feel?: An Interoceptive Moment with Your Neurobiological Self* (Princeton University Press, 2014).

15. H. D. Critchley, N. A. Harrison, Visceral Influences on Brain and Behavior. *Neuron* **77**, 624–638 (2013).

16. K. S. Quigley, S. Kanoski, W. M. Grill, L. F. Barrett, M. Tsakiris, Functions of Interoception: From Energy Regulation to Experience of the Self. *Trends in Neurosciences* **44**, 29–38 (2021).

17. I. R. Kleckner, *et al.*, Evidence for a large-scale brain system supporting allostasis and interoception in humans. *Nature Human Behaviour* **1**, 1–14 (2017).

18. G. G. Berntson, S. S. Khalsa, Neural Circuits of Interoception. *Trends in Neurosciences* **44**, 17–28 (2021).

19. H. C. Evrard, The Organization of the Primate Insular Cortex. *Front. Neuroanat.* **13**, 43 (2019).

20. P. J. Gianaros, L. K. Sheu, A review of neuroimaging studies of stressor-evoked blood pressure reactivity: Emerging evidence for a brain-body pathway to coronary heart disease risk. *NeuroImage* **47**, 922–936 (2009).

21. R. M. Harper, *et al.*, fMRI responses to cold pressor challenges in control and obstructive sleep apnea subjects. *Journal of Applied Physiology* **94**, 1583–1595 (2003).

22. A. B. Satpute, P. A. Kragel, L. F. Barrett, T. D. Wager, M. Bianciardi, Deconstructing arousal into wakeful, autonomic and affective varieties. *Neuroscience Letters* **693**, 19–28 (2019).

23. T. D. Wager, *et al.*, Brain mediators of cardiovascular responses to social threat: Part I: Reciprocal dorsal and ventral sub-regions of the medial prefrontal cortex and heart-rate reactivity. *NeuroImage* **47**, 821–835 (2009).

24. M. Zunhammer, T. Spisák, T. D. Wager, U. Bingel, Meta-analysis of neural systems underlying placebo analgesia from individual participant fMRI data. *Nat Commun* **12**, 1391 (2021).

25. J. Migeot, *et al.*, Allostatic-interoceptive anticipation of social rejection. *NeuroImage* **276**, 120200 (2023).

26. A. Birba, *et al.*, Allostatic-Interoceptive Overload in Frontotemporal Dementia. *Biological Psychiatry* **92**, 54–67 (2022).

27. A. L. Ruiz-Rizzo, *et al.*, Human subsystems of medial temporal lobes extend locally to amygdala nuclei and globally to an allostatic-interoceptive system. *NeuroImage* **207**, 116404 (2020).

28. G. M. Alvarez, M. D. Rudolph, J. R. Cohen, K. A. Muscatell, Lower Socioeconomic Position Is Associated with Greater Activity in and Integration within an Allostatic-Interoceptive Brain Network in Response to Affective Stimuli. *Journal of Cognitive Neuroscience* **34**, 1906–1927 (2022).

29. L. F. Barrett, A. B. Satpute, Large-scale brain networks in affective and social neuroscience: towards an integrative functional architecture of the brain. *Current Opinion in Neurobiology* **23**, 361–372 (2013).

30. M. L. Anderson, *After Phrenology: Neural Reuse and the Interactive Brain* (MIT Press, 2014).

31. B. T. T. Yeo, *et al.*, Functional Specialization and Flexibility in Human Association Cortex. *Cereb Cortex* **25**, 3654–3672 (2015).

32. D. Azzalini, I. Rebollo, C. Tallon-Baudry, Visceral Signals Shape Brain Dynamics and Cognition. *Trends in Cognitive Sciences* **23**, 488–509 (2019).

33. S. Cauzzo, *et al.*, Functional connectome of brainstem nuclei involved in autonomic, limbic, pain and sensory processing in living humans from 7 Tesla resting state fMRI. *NeuroImage* **250**, 118925 (2022).

34. R. N. Boubela, *et al.*, fMRI measurements of amygdala activation are confounded by stimulus correlated signal fluctuation in nearby veins draining distant brain regions. *Sci Rep* **5**, 10499 (2015).

35. M. Bianciardi, *et al.*, Toward an In Vivo Neuroimaging Template of Human Brainstem Nuclei of the Ascending Arousal, Autonomic, and Motor Systems. *Brain Connect* **5**, 597–607 (2015).

36. M. G. García-Gomar, *et al.*, In vivo Probabilistic Structural Atlas of the Inferior and Superior Colliculi, Medial and Lateral Geniculate Nuclei and Superior Olivary Complex in Humans Based on 7 Tesla MRI. *Frontiers in Neuroscience* **13** (2019).

37. M. G. García-Gomar, *et al.*, Disruption of Brainstem Structural Connectivity in REM Sleep Behavior Disorder Using 7 Tesla Magnetic Resonance Imaging. *Mov Disord* **37**, 847–853 (2022).

38. K. Singh, *et al.*, Probabilistic Template of the Lateral Parabrachial Nucleus, Medial Parabrachial Nucleus, Vestibular Nuclei Complex, and Medullary Viscero-Sensory-Motor Nuclei Complex in Living Humans From 7 Tesla MRI. *Frontiers in Neuroscience* **13** (2020).

39. K. Singh, M. G. García-Gomar, M. Bianciardi, Probabilistic Atlas of the Mesencephalic Reticular Formation, Isthmic Reticular Formation, Microcellular Tegmental Nucleus, Ventral Tegmental Area Nucleus Complex, and Caudal–Rostral Linear Raphe Nucleus Complex in Living Humans from 7 Tesla Magnetic Resonance Imaging. *Brain Connectivity* **11**, 613–623 (2021).

40. J. K. Harting, M. F. Huerta, T. Hashikawa, D. P. van Lieshout, Projection of the mammalian superior colliculus upon the dorsal lateral geniculate nucleus: Organization of tectogeniculate pathways in nineteen species. *Journal of Comparative Neurology* **304**, 275–306 (1991).

41. L. A. Benevento, J. H. Fallon, The ascending projections of the superior colliculus in the rhesus monkey (Macaca mulatta). *J Comp Neurol* **160**, 339–361 (1975).

42. A. J. Beitz, The organization of afferent projections to the midbrain periaqueductal gray of the rat. *Neuroscience* **7**, 133–159 (1982).

43. J. P. Card, R. Y. Moore, Organization of lateral geniculate-hypothalamic connections in the rat. *Journal of Comparative Neurology* **284**, 135–147 (1989).

44. J. D. Mikkelsen, A neuronal projection from the lateral geniculate nucleus to the lateral hypothalamus of the rat demonstrated with Phaseolus vulgaris leucoagglutinin tracing. *Neuroscience Letters* **116**, 58–63 (1990).

45. D. J. Uhlrich, J. B. Cucchiaro, S. M. Sherman, The projection of individual axons from the parabrachial region of the brain stem to the dorsal lateral geniculate nucleus in the cat. *J. Neurosci.* **8**, 4565–4575 (1988).

46. N. J. Gandhi, H. A. Katnani, Motor Functions of the Superior Colliculus. *Annu Rev Neurosci* **34**, 205–231 (2011).

47. T. Isa, E. Marquez-Legorreta, S. Grillner, E. K. Scott, The tectum/superior colliculus as the vertebrate solution for spatial sensory integration and action. *Current Biology* **31**, R741–R762 (2021).

48. K. A. Keay, P. Redgrave, P. Dean, Cardiovascular and respiratory changes elicited by stimulation of rat superior colliculus. *Brain Research Bulletin* **20**, 13–26 (1988).

49. N. Sahibzada, P. Dean, P. Redgrave, Movements resembling orientation or avoidance elicited by electrical stimulation of the superior colliculus in rats. *J. Neurosci.* **6**, 723–733 (1986).

50. A. Damasio, G. B. Carvalho, The nature of feelings: evolutionary and neurobiological origins. *Nat Rev Neurosci* **14**, 143–152 (2013).

51. A. Damasio, H. Damasio, D. Tranel, Persistence of Feelings and Sentience after Bilateral Damage of the Insula. *Cereb Cortex* **23**, 833–846 (2013).

52. M.-A. Coulombe, N. Erpelding, A. Kucyi, K. D. Davis, Intrinsic functional connectivity of periaqueductal gray subregions in humans: PAG Subregional Functional Connectivity. *Hum. Brain Mapp.* **37**, 1514–1530 (2016).

53. J. E. Iglesias, *et al.*, Bayesian longitudinal segmentation of hippocampal substructures in brain MRI using subject-specific atlases. *NeuroImage* **141**, 542–555 (2016).

54. H. F. Waguespack, B. L. Aguilar, L. Malkova, P. A. Forcelli, Inhibition of the Deep and Intermediate Layers of the Superior Colliculus Disrupts Sensorimotor Gating in Monkeys. *Frontiers in Behavioral Neuroscience* **14** (2020).

55. M. B. Parent, S. Higgs, L. G. Cheke, S. E. Kanoski, Memory and eating: A bidirectional relationship implicated in obesity. *Neuroscience & Biobehavioral Reviews* **132**, 110–129 (2022).

56. A. B. Satpute, *et al.*, Identification of discrete functional subregions of the human periaqueductal gray. *PNAS* **110**, 17101–17106 (2013).

57. L. J. Cronbach, N. Rajaratnam, G. C. Gleser, Theory of generalizability: A liberalization of reliability theory. *British Journal of Statistical Psychology* **16**, 137–163 (1963).

58. T. Yarkoni, Big Correlations in Little Studies: Inflated fMRI Correlations Reflect Low Statistical Power-Commentary on Vul et al. (2009). *Perspect Psychol Sci* **4**, 294–298 (2009).

59. A. L. Cohen, *et al.*, Defining functional areas in individual human brains using resting functional connectivity MRI. *Neuroimage* **41**, 45–57 (2008).

60. R. J. Morecraft, *et al.*, Cytoarchitecture and cortical connections of the anterior cingulate and adjacent somatomotor fields in the rhesus monkey. *Brain Res Bull* **87**, 457–497 (2012).

61. T. Chiba, T. Kayahara, K. Nakano, Efferent projections of infralimbic and prelimbic areas of the medial prefrontal cortex in the Japanese monkey, Macaca fuscata. *Brain Res* **888**, 83–101 (2001).

62. B. A. Vogt, D. N. Pandya, Cingulate cortex of the rhesus monkey: II. Cortical afferents. *J Comp Neurol* **262**, 271–289 (1987).

63. D. N. Pandya, G. W. Van Hoesen, M. M. Mesulam, Efferent connections of the cingulate gyrus in the rhesus monkey. *Exp Brain Res* **42**, 319–330 (1981).

64. M. P. van den Heuvel, O. Sporns, An Anatomical Substrate for Integration among Functional Networks in Human Cortex. *J. Neurosci.* **33**, 14489–14500 (2013).

65. X. An, R. Bandler, D. Ongür, J. L. Price, Prefrontal cortical projections to longitudinal columns in the midbrain periaqueductal gray in macaque monkeys. *J Comp Neurol* **401**, 455–479 (1998).

66. L. Jasmin, A. Granato, P. T. Ohara, Rostral agranular insular cortex and pain areas of the central nervous system: A tract-tracing study in the rat. *Journal of Comparative Neurology* **468**, 425–440 (2004).

67. X. Liu, *et al.*, The Superior Colliculus: Cell Types, Connectivity, and Behavior. *Neurosci. Bull.* **38**, 1519–1540 (2022).

68. Y. Katsumi, *et al.*, Correspondence of functional connectivity gradients across human isocortex, cerebellum, and hippocampus. *Commun Biol* **6**, 1–13 (2023).

69. R. Vos de Wael, *et al.*, Anatomical and microstructural determinants of hippocampal subfield functional connectome embedding. *Proceedings of the National Academy of Sciences* **115**, 10154–10159 (2018).

70. M. Bianciardi, *et al.*, In vivo functional connectome of human brainstem nuclei of the ascending arousal, autonomic, and motor systems by high spatial resolution 7-Tesla fMRI. *MAGMA* **29**, 451–462 (2016).

71. M. Xia, J. Wang, Y. He, BrainNet Viewer: A Network Visualization Tool for Human Brain Connectomics. *PLOS ONE* **8**, e68910 (2013).

72. H. W. Chase, A. A. Grace, P. T. Fox, M. L. Phillips, S. B. Eickhoff, Functional differentiation in the human ventromedial frontal lobe: A data-driven parcellation. *Human Brain Mapping* **41**, 3266–3283 (2020).

73. F. Jin, P. Zheng, H. Liu, H. Guo, Z. Sun, Functional and anatomical connectivity-based parcellation of human cingulate cortex. *Brain and Behavior* **8**, e01070 (2018).

74. N. Palomero-Gallagher, *et al.*, Human Pregenual Anterior Cingulate Cortex: Structural, Functional, and Connectional Heterogeneity. *Cerebral Cortex (New York, NY)* **29**, 2552 (2019).

75. E. T. Rolls, *et al.*, Functional Connectivity of the Anterior Cingulate Cortex in Depression and in Health. *Cerebral Cortex* **29**, 3617–3630 (2019).

76. C. Yu, *et al.*, Functional segregation of the human cingulate cortex is confirmed by functional connectivity based neuroanatomical parcellation. *NeuroImage* **54**, 2571–2581 (2011).

77. F. Cauda, *et al.*, Functional connectivity of the insula in the resting brain. *NeuroImage* **55**, 8–23 (2011).

78. L. J. Chang, T. Yarkoni, M. W. Khaw, A. G. Sanfey, Decoding the Role of the Insula in Human Cognition: Functional Parcellation and Large-Scale Reverse Inference. *Cerebral Cortex* **23**, 739–749 (2013).

79. B. Deen, N. B. Pitskel, K. A. Pelphrey, Three Systems of Insular Functional Connectivity Identified with Cluster Analysis. *Cerebral Cortex* **21**, 1498–1506 (2011).

80. C. Kelly, *et al.*, A convergent functional architecture of the insula emerges across imaging modalities. *NeuroImage* **61**, 1129–1142 (2012).

81. K.-J. Bär, *et al.*, Functional connectivity and network analysis of midbrain and brainstem nuclei. *Neuroimage* **134**, 53–63 (2016).

82. K. Singh, *et al.*, Functional connectome of arousal and motor brainstem nuclei in living humans by 7 Tesla resting-state fMRI. *NeuroImage* **249**, 118865 (2022).

83. S. Demeter, D. L. Rosene, G. W. van Hoesen, Interhemispheric pathways of the hippocampal formation, presubiculum, and entorhinal and posterior parahippocampal cortices in the rhesus monkey: The structure and organization of the hippocampal commissures. *Journal of Comparative Neurology* **233**, 30–47 (1985).

84. Y. Kobayashi, D. G. Amaral, Macaque monkey retrosplenial cortex: III. Cortical efferents. *Journal of Comparative Neurology* **502**, 810–833 (2007).

85. C. R. Olson, S. Y. Musil, Topographic organization of cortical and subcortical projections to posterior cingulate cortex in the cat: Evidence for somatic, ocular, and complex subregions. *Journal of Comparative Neurology* **324**, 237–260 (1992).

86. P. Y. Risold, R. H. Thompson, L. W. Swanson, The structural organization of connections between hypothalamus and cerebral cortex. *Brain Res Brain Res Rev* **24**, 197–254 (1997).

87. J. Zhang, *et al.*, Topography Impacts Topology: Anatomically Central Areas Exhibit a "High-Level Connector" Profile in the Human Cortex. *Cereb Cortex* **30**, 1357–1365 (2020).

88. M. Tsanov, Differential and complementary roles of medial and lateral septum in the orchestration of limbic oscillations and signal integration. *European Journal of Neuroscience* **48**, 2783–2794 (2018).

89. Y. Takeuchi, *et al.*, The Medial Septum as a Potential Target for Treating Brain Disorders Associated With Oscillopathies. *Frontiers in Neural Circuits* **15** (2021).

90. G. T. Cottrell, A. V. Ferguson, Sensory circumventricular organs: central roles in integrated autonomic regulation. *Regulatory Peptides* **117**, 11–23 (2004).

91. C. J. Price, T. D. Hoyda, A. V. Ferguson, The area postrema: a brain monitor and integrator of systemic autonomic state. *Neuroscientist* **14**, 182–194 (2008).

92. M. A. Karim, S. K. Leong, S. A. Perwaiz, On the anatomical organization of the vagal nuclei. *American Journal of Primatology* **1**, 277–292 (1981).

93. M. Kalia, M. M. Mesulam, Brain stem projections of sensory and motor components of the vagus complex in the cat: II. Laryngeal, tracheobronchial, pulmonary, cardiac, and gastrointestinal branches. *J Comp Neurol* **193**, 467–508 (1980).

94. R. S. Maior, *et al.*, A role for the superior colliculus in the modulation of threat responsiveness in primates: toward the ontogenesis of the social brain. *Reviews in the Neurosciences* **23**, 697–706 (2012).

95. T. L. Davidson, *et al.*, Hippocampal lesions impair retention of discriminative responding based on energy state cues. *Behavioral Neuroscience* **124**, 97–105 (2010).

96. J. L. Gauthier, D. W. Tank, A Dedicated Population for Reward Coding in the Hippocampus. *Neuron* **99**, 179-193.e7 (2018).

97. S. E. Kanoski, H. J. Grill, Hippocampus Contributions to Food Intake Control: Mnemonic, Neuroanatomical, and Endocrine Mechanisms. *Biological Psychiatry* **81**, 748–756 (2017).

98. E. E. Noble, *et al.*, Hypothalamus-hippocampus circuitry regulates impulsivity via melanin-concentrating hormone. *Nat Commun* **10**, 4923 (2019).

99. D. Zeithamova, B. D. Gelman, L. Frank, A. R. Preston, Abstract Representation of Prospective Reward in the Hippocampus. *J. Neurosci.* **38**, 10093–10101 (2018).

100. C. Shaffer, L. F. Barrett, K. S. Quigley, Signal Processing in the Vagus Nerve: Hypotheses Based on New Genetic and Anatomical Evidence (In prep).

101. M. Brændholt, *et al.*, Breathing in waves: Understanding respiratory-brain coupling as a gradient of predictive oscillations. *Neuroscience & Biobehavioral Reviews* **152**, 105262 (2023).

102. L. P. Morin, J. H. Blanchard, Forebrain connections of the hamster intergeniculate leaflet: Comparison with those of ventral lateral geniculate nucleus and retina. *Vis Neurosci* **16**, 1037–1054 (1999).

103. R. Y. Moore, R. Weis, M. M. Moga, Efferent projections of the intergeniculate leaflet and the ventral lateral geniculate nucleus in the rat. *Journal of Comparative Neurology* **420**, 398–418 (2000).

104. H. C. Hughes, W. H. Mullikin, Brainstem afferents to the lateral geniculate nucleus of the cat. *Exp Brain Res* **54** (1984).

105. L. F. Barrett, K. S. Quigley, P. Hamilton, An active inference theory of allostasis and interoception in depression. *Philos Trans R Soc Lond B Biol Sci* **371**, 20160011 (2016).

106. C. Shaffer, C. Westlin, K. S. Quigley, S. Whitfield-Gabrieli, L. F. Barrett, Allostasis, Action, and Affect in Depression: Insights from the Theory of Constructed Emotion. *Annu Rev Clin Psychol* **18**, 553–580 (2022).

107. M. Ardizzi, *et al.*, Interoception and Positive Symptoms in Schizophrenia. *Frontiers in Human Neuroscience* **10** (2016).

108. B. Yao, K. Thakkar, Interoception abnormalities in schizophrenia: A review of preliminary evidence and an integration with Bayesian accounts of psychosis. *Neurosci Biobehav Rev* **132**, 757–773 (2022).

109. D. DuBois, S. H. Ameis, M.-C. Lai, M. F. Casanova, P. Desarkar, Interoception in Autism Spectrum Disorder: A review. *International Journal of Developmental Neuroscience* **52**, 104–111 (2016).

110. K. B. Schauder, L. E. Mash, L. K. Bryant, C. J. Cascio, Interoceptive ability and body awareness in autism spectrum disorder. *Journal of Experimental Child Psychology* **131**, 193–200 (2015).

111. I. García-Cordero, *et al.*, Feeling, learning from and being aware of inner states: interoceptive dimensions in neurodegeneration and stroke. *Philosophical Transactions of the Royal Society B: Biological Sciences* **371**, 20160006 (2016).

112. C. R. Marshall, *et al.*, Impaired Interoceptive Accuracy in Semantic Variant Primary Progressive Aphasia. *Frontiers in Neurology* **8** (2017).

113. L. Ricciardi, *et al.*, Know thyself: Exploring interoceptive sensitivity in Parkinson's disease. *Journal of the Neurological Sciences* **364**, 110–115 (2016).

114. G. Santangelo, *et al.*, Interoceptive processing deficit: A behavioral marker for subtyping Parkinson's disease. *Parkinsonism & Related Disorders* **53**, 64–69 (2018).

115. A. Yoris, *et al.*, Multicentric evidence of emotional impairments in hypertensive heart disease. *Sci Rep* **10**, 14131 (2020).

116. D. Di Lernia, M. Lacerenza, V. Ainley, G. Riva, Altered Interoceptive Perception and the Effects of Interoceptive Analgesia in Musculoskeletal, Primary, and Neuropathic Chronic Pain Conditions. *Journal of Personalized Medicine* **10**, 201 (2020).

117. B. Bonaz, *et al.*, Diseases, Disorders, and Comorbidities of Interoception. *Trends in Neurosciences* **44**, 39–51 (2021).

118. S. S. Khalsa, *et al.*, Interoception and Mental Health: A Roadmap. *Biol Psychiatry Cogn Neurosci Neuroimaging* **3**, 501–513 (2018).

119. G. Locatelli, *et al.*, What is the role of interoception in the symptom experience of people with a chronic condition? A systematic review. *Neuroscience & Biobehavioral Reviews* **148**, 105142 (2023).

120. J. P. Hamilton, M. Farmer, P. Fogelman, I. H. Gotlib, Depressive Rumination, the Default-Mode Network, and the Dark Matter of Clinical Neuroscience. *Biological Psychiatry* **78**, 224–230 (2015).

121. H.-X. Zhou, *et al.*, Rumination and the default mode network: Meta-analysis of brain imaging studies and implications for depression. *NeuroImage* **206**, 116287 (2020).

122. L. Q. Uddin, *et al.*, Salience Network–Based Classification and Prediction of Symptom Severity in Children With Autism. *JAMA Psychiatry* **70**, 869–879 (2013).

123. M. N. Baliki, A. R. Mansour, A. T. Baria, A. V. Apkarian, Functional Reorganization of the Default Mode Network across Chronic Pain Conditions. *PLOS ONE* **9**, e106133 (2014).

124. H. Chen, *et al.*, Shared atypical default mode and salience network functional connectivity between autism and schizophrenia. *Autism Research* **10**, 1776–1786 (2017).

125. S. C. de Lange, *et al.*, Shared vulnerability for connectome alterations across psychiatric and neurological brain disorders. *Nat Hum Behav* **3**, 988–998 (2019).

126. G. E. Doucet, *et al.*, Transdiagnostic and disease-specific abnormalities in the default-mode network hubs in psychiatric disorders: A meta-analysis of resting-state functional imaging studies. *European Psychiatry* **63**, e57 (2020).

127. C.-C. Huang, *et al.*, Transdiagnostic and Illness-Specific Functional Dysconnectivity Across Schizophrenia, Bipolar Disorder, and Major Depressive Disorder. *Biological Psychiatry: Cognitive Neuroscience and Neuroimaging* **5**, 542–553 (2020).

128. C. L. Nord, S. N. Garfinkel, Interoceptive pathways to understand and treat mental health conditions. *Trends in Cognitive Sciences* **26**, 499–513 (2022).

129. C. C. C. Bauer, *et al.*, Real-time fMRI neurofeedback reduces auditory hallucinations and modulates resting state connectivity of involved brain regions: Part 2: Default mode network -preliminary evidence. *Psychiatry Res* **284**, 112770 (2020).

130. J. Zhang, *et al.*, Reducing default mode network connectivity with mindfulness-based fMRI neurofeedback: a pilot study among adolescents with affective disorder history. *Mol Psychiatry*, 1–9 (2023).

131. J. Cesario, D. J. Johnson, H. L. Eisthen, Your Brain Is Not an Onion With a Tiny Reptile Inside. *Curr Dir Psychol Sci* **29**, 255–260 (2020).

132. L. Chanes, L. F. Barrett, Redefining the Role of Limbic Areas in Cortical Processing. *Trends in Cognitive Sciences* **20**, 96–106 (2016).

133. M. M. Mesulam, From sensation to cognition. *Brain* **121**, 1013–1052 (1998).

134. C. L. Zold, M. G. H. Shuler, Theta Oscillations in Visual Cortex Emerge with Experience to Convey Expected Reward Time and Experienced Reward Rate. *J. Neurosci.* **35**, 9603–9614 (2015).

135. A. B. Satpute, *et al.*, Involvement of Sensory Regions in Affective Experience: A Meta-Analysis. *Front Psychol* **6**, 1860 (2015).

136. P. Vuilleumier, How brains beware: neural mechanisms of emotional attention. *Trends Cogn Sci* **9**, 585–594 (2005).

137. M. Allen, *et al.*, Anterior insula coordinates hierarchical processing of tactile mismatch responses. *Neuroimage* **127**, 34–43 (2016).

138. R. A. Baer, G. T. Smith, K. B. Allen, Assessment of Mindfulness by Self-Report: The Kentucky Inventory of Mindfulness Skills. *Assessment* **11**, 191–206 (2004).